Electronic Supplementary Material (ESI) for Chemical Communications.

SUPPORTING INFORMATION

Pd-NiO-Y/CNT Nanofoam: A Zeolite-Carbon Nanotube Conjugal Exhibiting High Durability in Methanol Oxidation

Mukesh Sharma[a], Biraj Das[a], Manash J. Baruah[a], Pradip K. Bhattacharyya[b], Lakshi Saikia[c] and Kusum K Bania*[a]

[a]*Department of Chemical Sciences, Tezpur university, Assam-784028, India*

[b]*Department of Chemistry, Arya Vidyapeeth College, Guwahati, Assam, India, 781016*

[c]*Materials Science Division, CSIR-North East Institute of Science and Technology, Jorhat 785006, Assam, India.*

Corresponding Authors

*E-mail: kusum@tezu.ernet.in.

ORCID: 0000-0001-6535-3913

Experimental Section

1.1. Materials. Palladium chloride pure, $PdCl_2$ and Nickel (II) chloride hexahydrate, $NiCl_2.6H_2O$ were purchased from SRL and were used as a source of palladium and nickel, respectively. Zeolite-Y, Multi-Walled Carbon Nano Tube (MWCNT) and Nafion solution were obtained from Sigma Aldrich. Sodium hydroxide (NaOH) was received from E-Merck. Deionized water was used for the preparation of 1 M NaOH. Dried methanol was brought from E-Merck for methanol oxidation reaction (MOR). The commercial Pd/C was purchased from Sigma Aldrich.

1.2. Synthesis of Palladium Oxide zeolite-Y, PdO-Y, Nickel Oxide zeolite-Y, NiO-Y and Pd-NiO-Y. The preparation of these materials are already reported in our previous work and we follow the same approach to get the materials for methanol oxidation reaction.[1]

1.3. Synthesis of hybridized Pd-NiO-Y/CNT. To the prepared Pd-NiO-Y catalyst followed by the reported procedure,[1] 0.05 g of MWCNT was added and the mixture was taken in a mortar and ground for 2-3 hours. Small aliquot of water was used during grinding and the mixture was heated at 120 ˚C for certain intervals of time. The process of grinding and heating continued for almost 50-60 hours, which resulted in the change of colour from light brown to chocolate brown. Finally the solid material was washed for a number of times with deionized water and dried before subjecting to characterization.

1.4. Physical Measurement. The Transmission Electron Microscopy (TEM) analysis was carried out using a JEM-2010 (JEOL) instrument operational with a slow-scan CCD camera and with an accelerating voltage of 200kV. High resolution TEM (HRTEM) and elemental mapping and energy dispersive X-ray (EDX) analysis was performed on JEM 2100 Plus (JEOL). X-ray diffraction (XRD) analysis were performed in a BRUKER AXS, D8 FOCUS instrument and low angle measurement from 5-80°. The Raman signal of the samples was taken by an EZRaman-N (EnwaveOptronics) Raman spectrometer. Laser light of 150 mW, 514 nm incident wavelength through a 100x (0.3 N.A.) objective lens was used to excite all the samples.The XPS of the sample was measured using Mg Kα (1253.6 eV) radiation as a source on a KRATOS (ESCA AXIS 165) spectrometer. The oven-dried samples (finely ground) were dusted on a graphite sheet (double stick) and mounted over the regular sample holder, before being transferred to an analysis chamber. Before recording the XPS, the material was outgassed overnight in a vacuum oven. The binding energy values were corrected with reference to C (1s) peak at 284.8 eV and the peaks were deconvoluted using Origin software. The BET surface areas were determined using N_2 sorption data calculated at 77 K employing volumetric adsorption setup (NOVA 1000e, Quantachrome Instruments). Pore diameters of sample was determined from desorption branch of N_2 adsorption isotherm employing Barret, Joyner, and Halenda (BJH) method. The cyclic voltammetry (CV) studies were performed in a CHI-600E meter from CH Instruments using the glassy carbon electrode (GCE) as a working electrode, Ag/AgCl as reference electrode and Pt wire as a counter electrode, respectively. Infra-red spectra (FTIR) in the range of 500-4000 cm^{-1} were recorded on a Perkin-Elmer Spectrum 2000 FTIR spectrometer. FTIR spectra of the solid materials were recorded against a zeolite background, which was recorded after 1 h of evacuation.

1.5. Electrochemical measurements. Three electrode systems consisting of glassy carbon electrode (GCE) as working electrode, Ag/AgCl electrode as reference and a platinum wire as the counter electrode, respectively was assembled for methanol oxidation reaction (MOR). For modification of the GCE electrode, the electrocatalyst was prepared by mixing 1 mg of synthesized Pd-NiO-Y/CNT and 1mL of Nafion (0.2% w/w) solution followed by addition of 1mL of ethanol/H_2O solution. The obtained paste was sonicated continuously for 60 min until a homogeneous ink was formed. From the obtained ink a certain aliquot was drop casted on GCE and dried in air to get a uniform surface. The cyclic voltammograms were run in alkaline medium using 1M NaOH. Diameter of GCE was 3 mm and the catalyst loading was 300 μg/cm^{-2}, Pd-content in the loaded catalyst (Pd-NiO-Y/CNT) was 25.7 μg/cm^{-2}.

The Electrochemical Impedance measurements (EIS) were performed in the CHI-600E meter from CH Instruments using conventional three-component electrode systems. EIS was conducted with voltage amplitude of 0.1 V and a frequency range of 1Hz to1MHz.

Linear sweep voltammetry (LSV) measurements were performed on two samples *viz* Pd-NiO-Y/CNT and Pd-NiO-Y to see the CO-oxidation peak upon saturating with pure CO gas. Following the reported procedure by Xu *et al.*[2] the electrolyte was saturated with highly pure carbon monoxide (CO) gas by bubbling with CO to form a monolayer on the GCE. The excess of CO was removed by passing argon (Ar) gas for 20 min. The oxidation peak of the CO adsorbed peak was detected by performing LSV at a scan rate of 20 mV/s. The electrochemically active surface area (ECSA) was estimated by integrating the peak area of oxidizing CO_{ad}. The ECSA of the samples were calculated using the following formula

ECSA= Q/m*C where in which Q is the charge calculated from the peak area of the oxidation peak, m is the amount of Pd-loading; C is the charge (420 μC cm^{-2}) required for CO monolayer formation.[3]

1.6. Computational details: DFT calculations are carried out using Becke three-parameter exchange and Lee, Yang and Parr correlation functional B3LYP functional and 6-31++g(d,p) basis set for C O H Si Ni and DGDZVP for Pd. Calculations are performed using a Gaussian 09.[4]

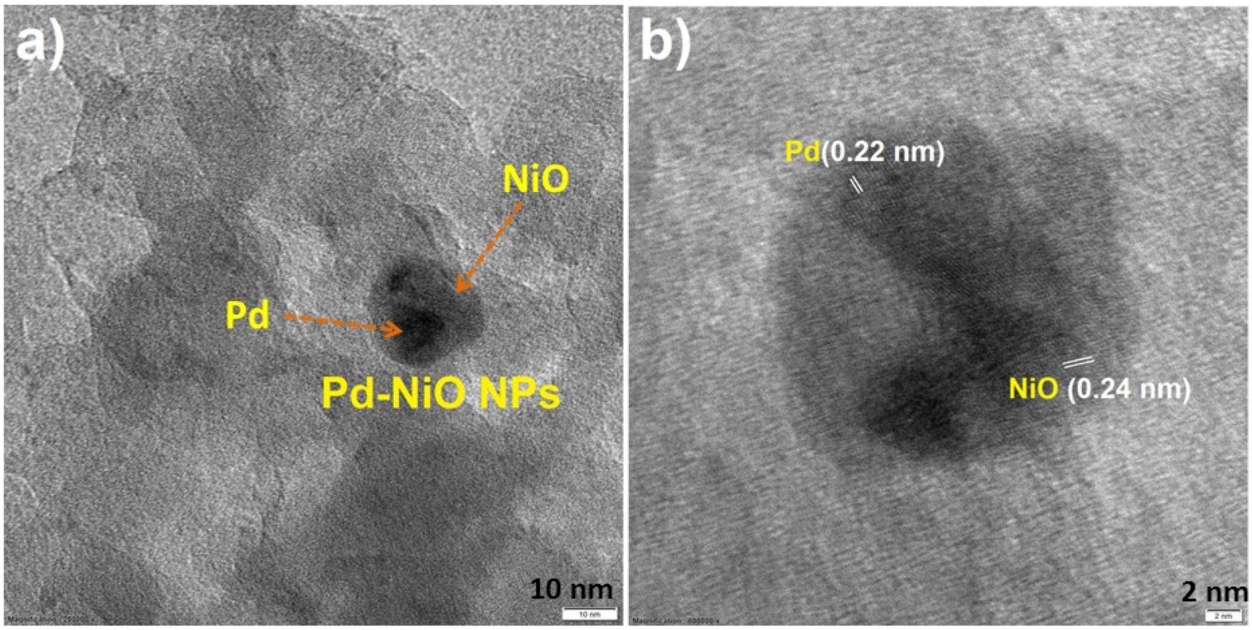

Fig. S1 a,b**)** HRTEM images of a single Pd-NiO NPs displaying characteristics lattice fringe patterns for Pd and NiO.

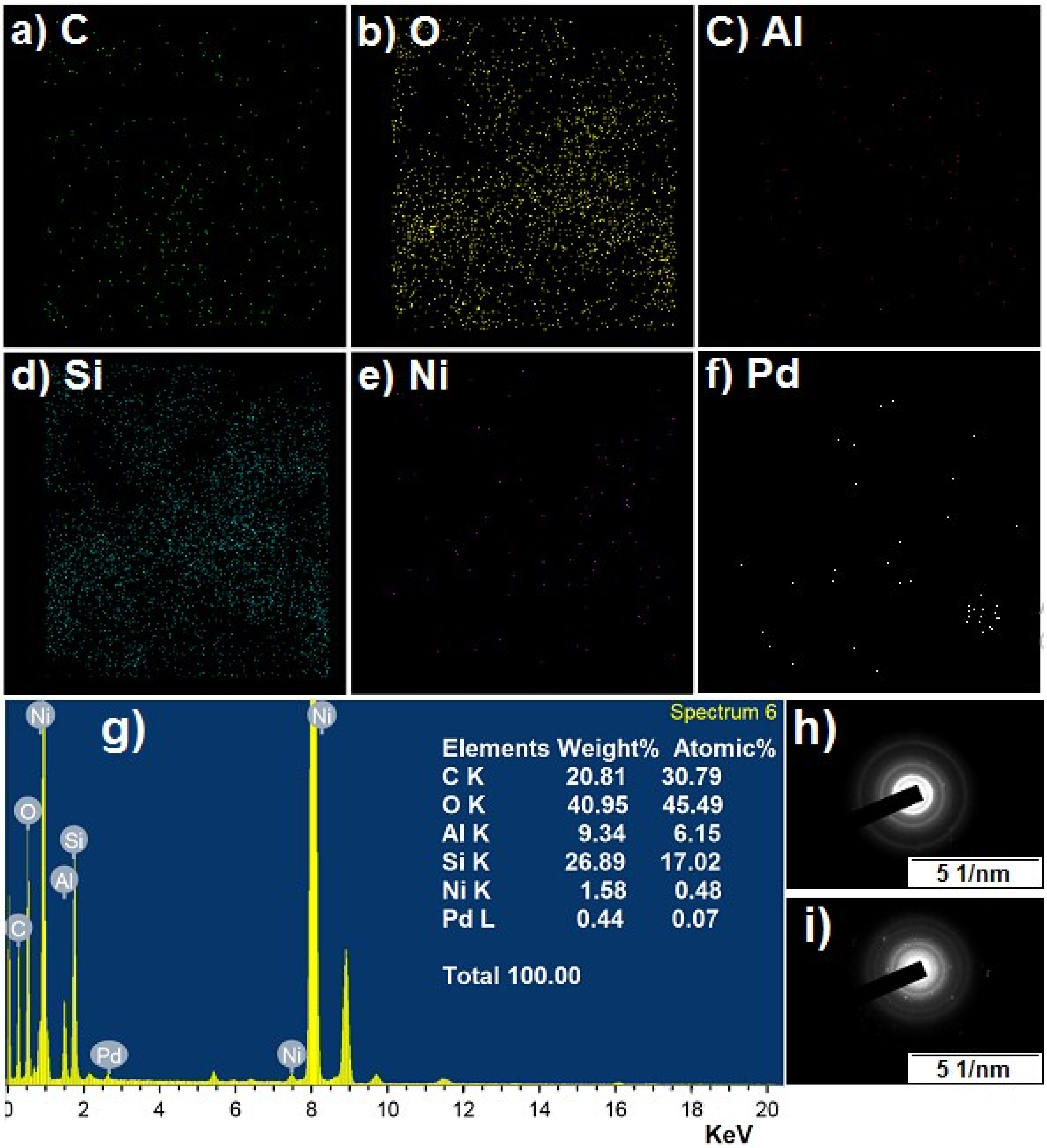

Fig. S2 a-f) HRTEM elemental mapping of the Pd-NiO-Y/CNT showing the presence of a) C, b) O, c) Al, d) Si, e) Ni, f) Pd, g) TEM-EDX spectra displaying different compositions of the elements, and h,i) are the SAED patterns of the nanocomposite.

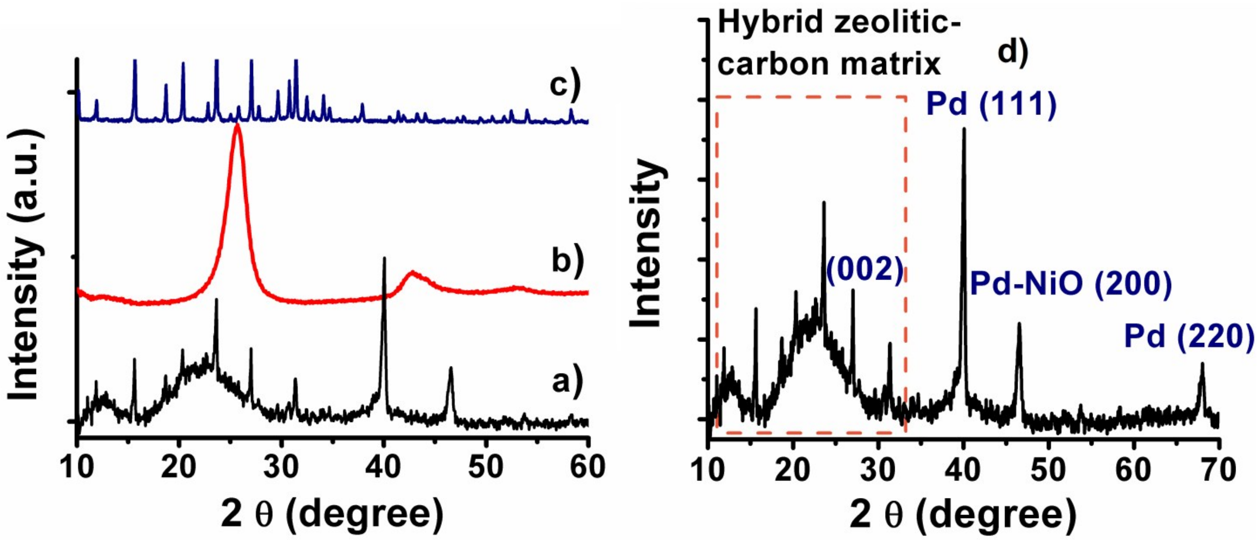

Fig. S3 XRD patterns of a), Pd-NiO-Y/CNT, b) neat MWCNT, c) neat zeolite-Y, and d) Pd-NiO-Y/CNT in the range 10-70˚ 2θ values.

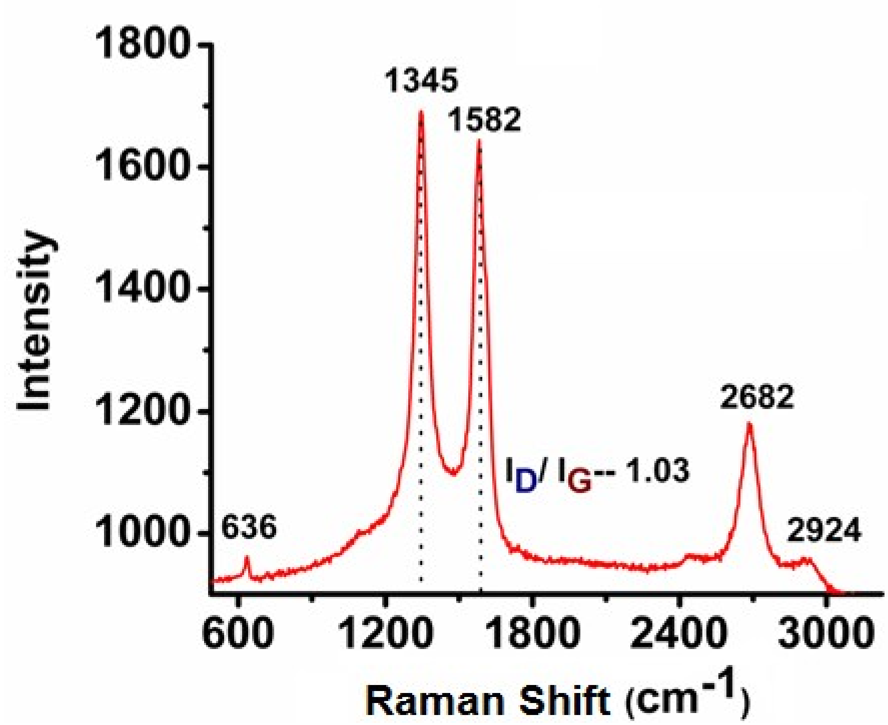

Fig. S4 Raman spectra of hybrid Pd-NiO-Y/CNT.

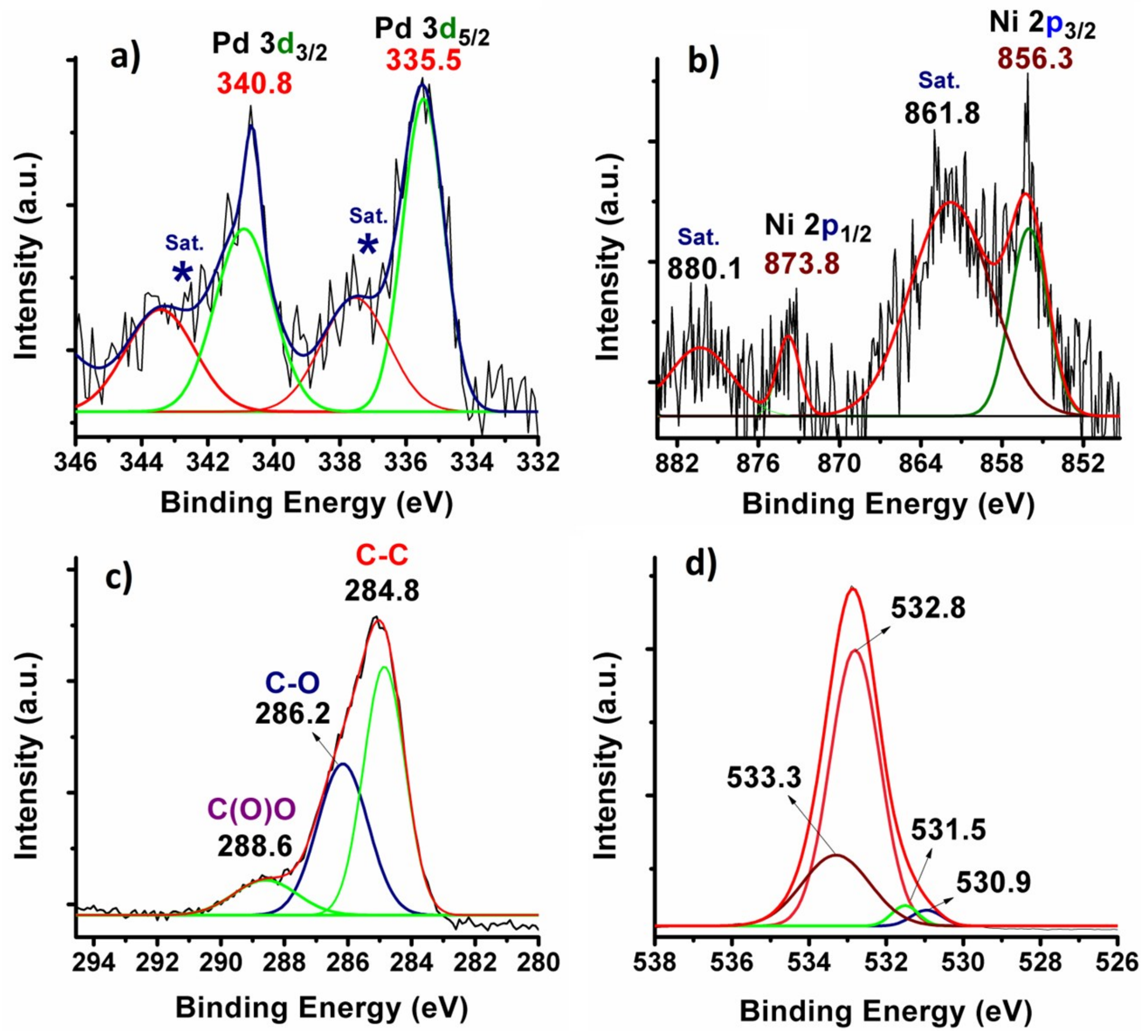

Fig. S5 XPS spectra of Pd-NiO-Y/CNT nanocomposite displaying binding energy values in electron volt (eV) for (a) Pd 3d, (b) Ni 2p, (c) C 1s, and (d) O 1s regions.

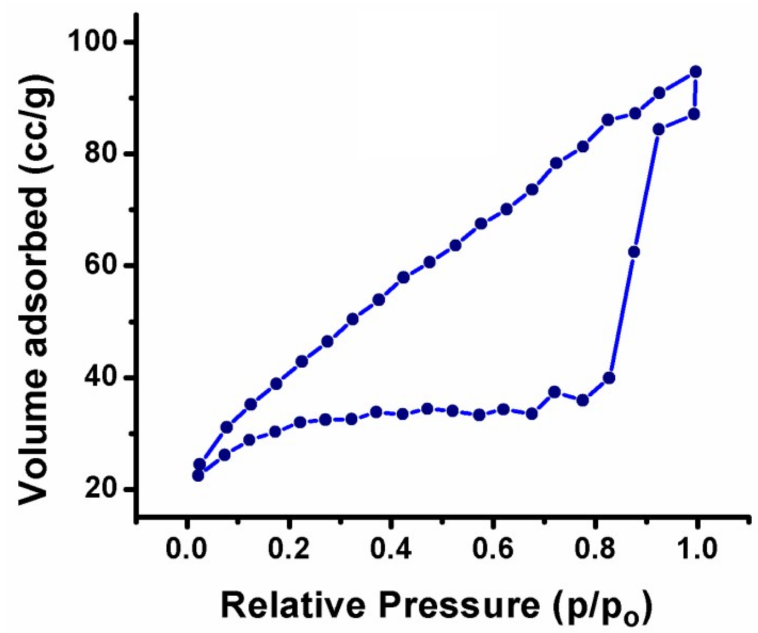

Fig. S6 The nitrogen adsorption-desorption isotherm of hybrid Pd-NiO-Y/CNT nanocomposite.

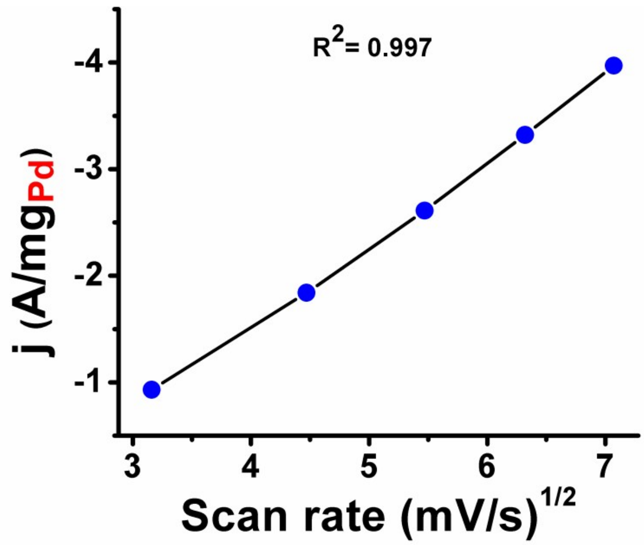

Fig. S7 Plot of variation of current density vs. square root of scan rate $(mV/s)^{1/2}$.

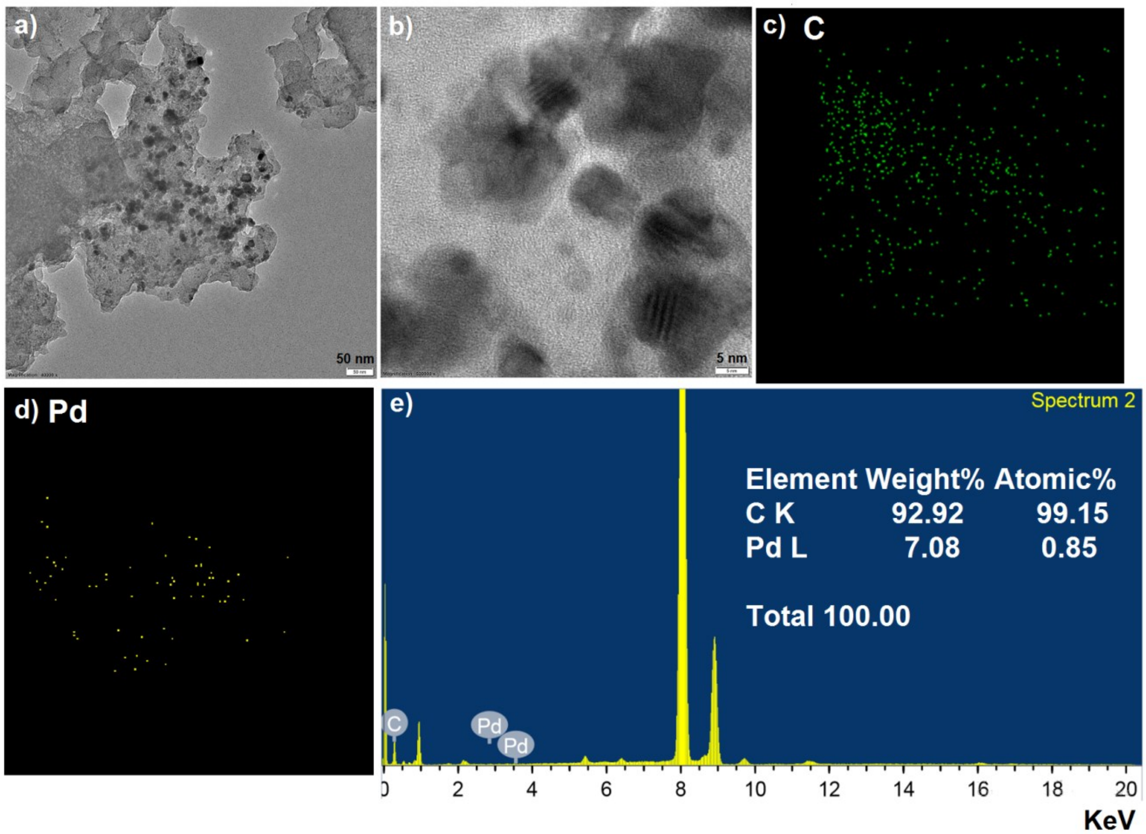

Fig. S8 a,b) TEM images and elemental mapping of commercial Pd/C showing the presence of c) C, d) Pd, and e) TEM-EDX spectra displaying the compositions of C and Pd.

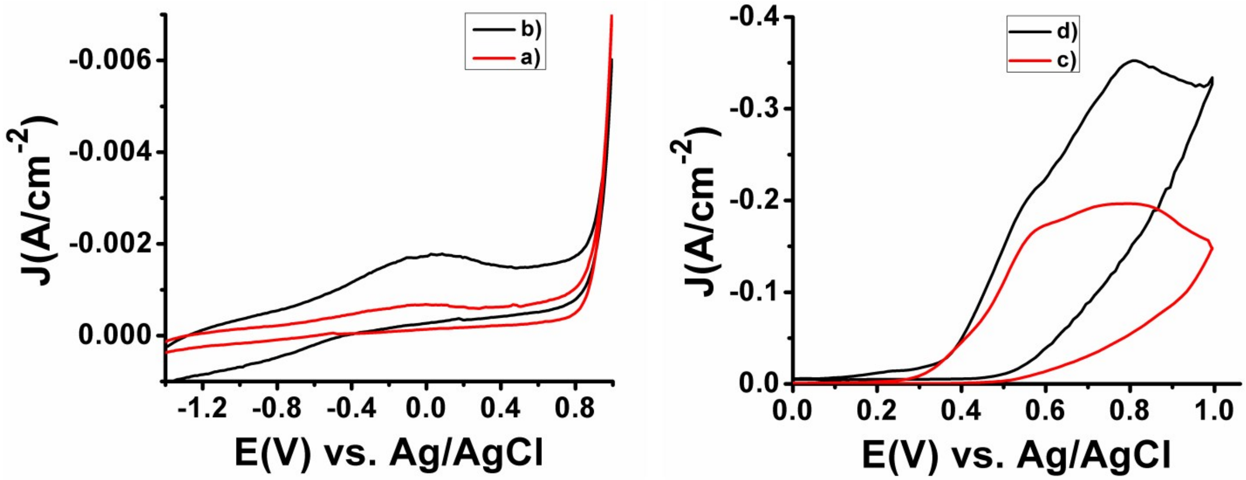

Fig. S9 MOR performed under identical conditions with commercial Pd/C employing a) 2 mL, b) 4 mL of 1 M methanol and with synthesized NiO-Y/CNT using c) 2 mL and d) 4 mL of methanol.

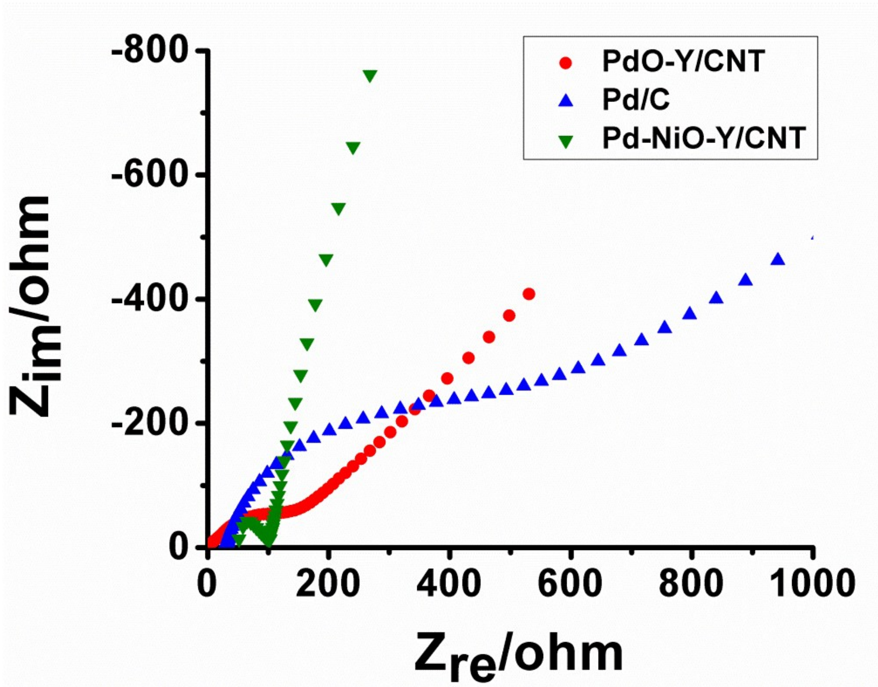

Fig. S10 Nyquist plots of MOR with PdO-Y/CNT (red), commercial Pd/C (blue) and Pd-NiO-Y/CNT (green) catalysts.

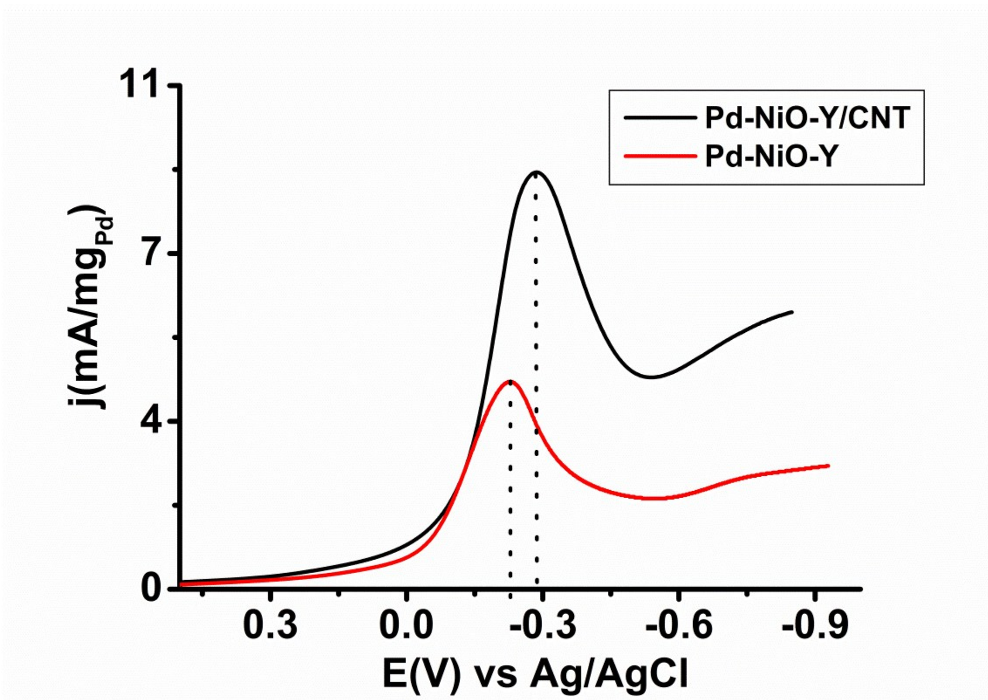

Fig. S11 Linear sweep voltammetry (LSV) curves for the oxidation peaks of Pd-NiO-Y (red) and Pd-NiO-Y/CNT (black) after adsorption of saturated CO.

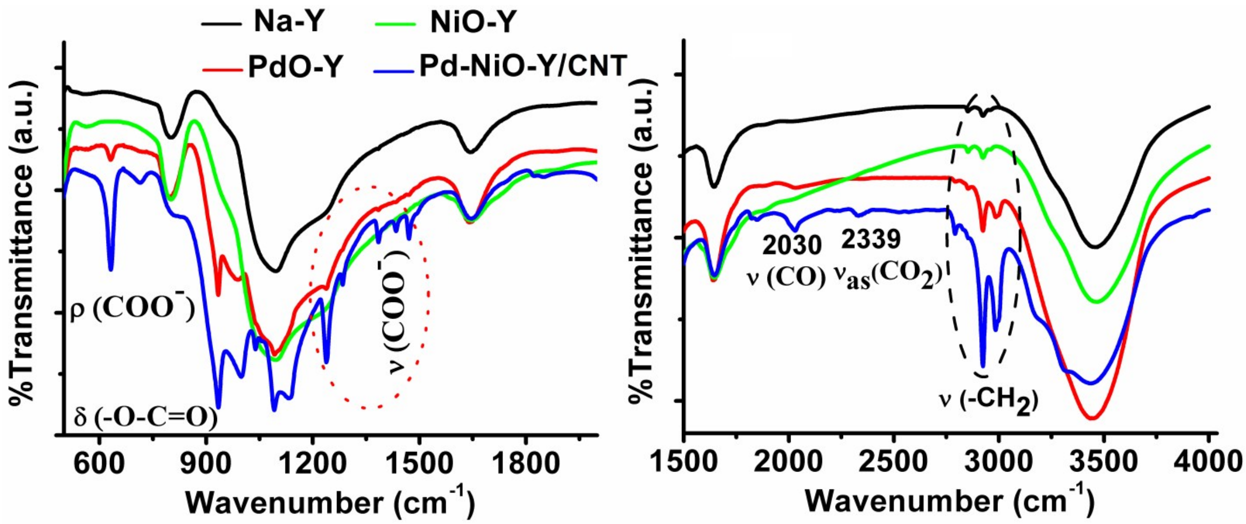

Fig. 12 FT-IR spectra showing the formation of various species during CH_3OH oxidation over different catalyst surface.

1.7. DFT-Analysis: In order to understand the mechanism of CH_3OH oxidation over Pd-NiO-Y surface, a simple framework comprising of Pd, Ni, and Si was considered for density functional theory (DFT) calculation. As understood from various literatures,[5-7] the oxidation of CH_3OH over metal-oxide surface can proceed through direct C-H bond activation process or by indirect O-H bond-breaking favouring the C-H bond activation. Sheng *et al.*[8a] with RuO_2 observed the direct process to be energetically unfavorable and accordingly we also did not succeeded with the direct activation process. However, similar to their results we also found the alcoholic OH hydrogen abstraction process through indirect O–H bond breaking to be highly favourable with the reaction energy of 0 eV.[8a] Therefore; we considered the indirect pathway and optimized the possible species that might have generated during the oxidation reaction. The CH_3OH was believed to get adsorbed on the catalyst surface through Pd-O bond interaction (Fig S13a). The Pd-O distance at this stage was found to be 1.96 Å. As the reaction was base (NaOH) assisted, so probably the OH^- ions from the base got adsorbed on the catalyst surface and abstracted the O-H proton of CH_3OH leaving behind CH_3O* species with the generation of water molecule. (Fig. S13b). Once the CH_3O* species is formed, the C-H bond activation process becomes easier, and the process of deprotonation of methanol continues until it got completely oxidized to CO_2 and H_2O *via* the formation of various species mostly HCHO and HCOOH. The optimized geometries of the formation of HCHO and HCOOH are depicted in Fig. S13c, d. The abstraction process was found to be barrier less. Different geometries of the alcoholic hydrogen abstraction by the base OH^- along with changes in O-H and Pd-O distances are depicted in Fig. S14 (a-c).

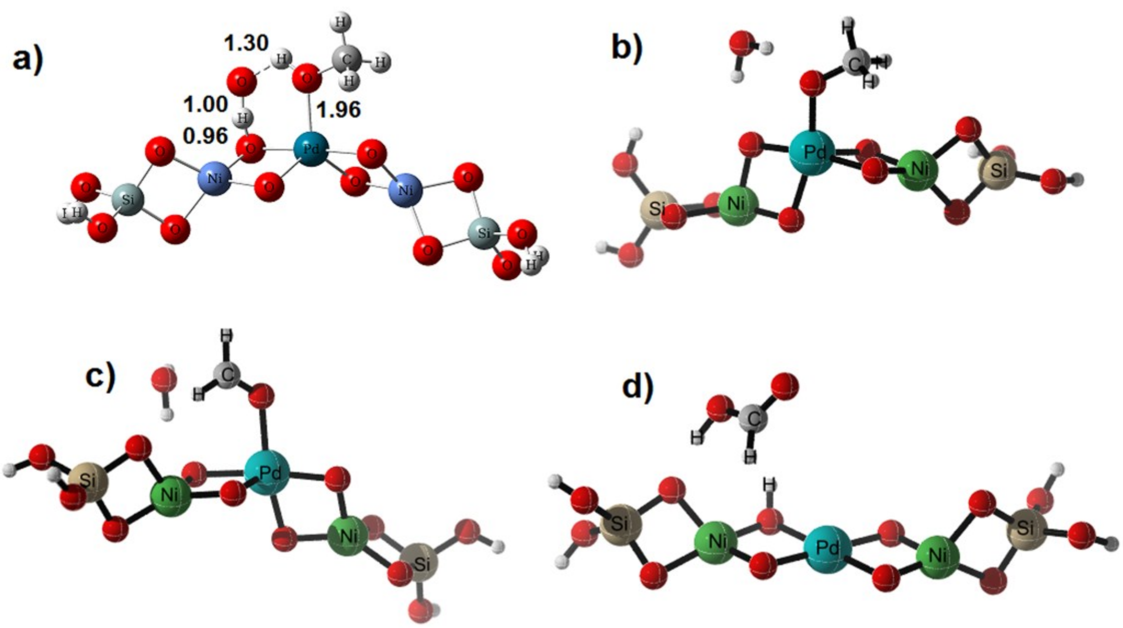

Fig. S13 Optimized geometries showing (a) interaction of CH_3OH with Pd through OH group and surface binding of OH^-, (b) generation of CH_3O^* and H_2O and its stabilization over catalyst surface, (c) and (d) formation of HCHO and HCOOH after proton abstraction from CH_3O^*.

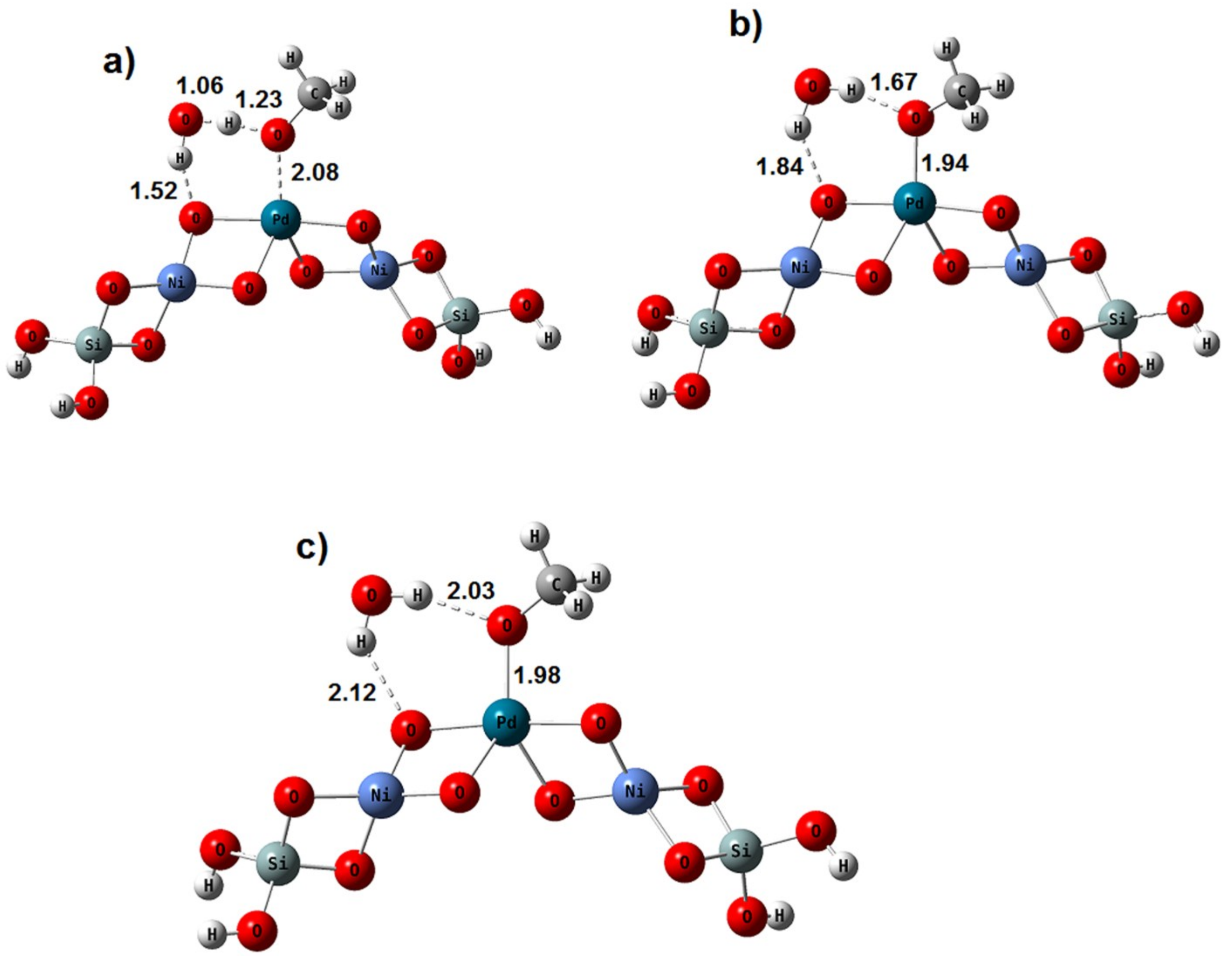

Fig. S14 (a-c) Steps involves in proton abstraction from CH_3OH bound to Pd-NiO-Y by surface bound OH^-.

Table S1 BET analysis results for neat zeolite-NaY and hybridized Pd-NiO-Y/CNT.

Sl. No.	Compound	BJH pore size (in Å)	Pore volume (cc/g)	BET surface area (m^2/g)
1.	Na-Y	6.20	0.30	645[8b]
2.	Pd-NiO-Y/CNT	72.8	0.182	346.6

Table S2 Comparison of the various reported Pd-Ni-based electrocatalysts along with their synthesis methods, anodic current densities and durability in methanol oxidation reaction.

Sl No	Electrocatalysts	Methods	Anodic Current density	Durability	Ref.
1	Ni@Pd CS	$NaBH_4$, SDS etc.	770.7 $mAmg^{-1}Pd$	120 min	9
2	PdNi/RGO/POM	Wet-chemical method	1223.6 mA $mg^{-1}Pd$	4000 s	10
3	PdNi/C	Chemical reduction	530 mA mg^{-1} Pd	-	11
4	Pd/NiO NP	Dealloying method	344 mA $mg^{-1}Pd$	3000 s	12
5	Ni@Pd/MWCNT	Impregnation and replacement method	~32 mA cm^{-2}	-	13
6	PdNiNSs	$NaBH_4$	677.08 mA mg^{-1}	500 cycle	14
7	PdNi alloy	Dealloying method	75-95 mA cm^{-2} Pd	-	15
8	Pd/PdNi/C	Chemical reduction	~40-90 Ag^{-1} Pd	-	16
9	$PdNi/TiO_2$	Deposition method	-	-	17
10	PdNi/carbon	Impregnation, $NaBH_4$	7.64 mA cm^{-2}	80 min	18
11	Ni–Pd/Si-MCP	Electroless plating	0.36 A cm^{-2}	600s	19
12	Pd-4-Ni	Galvanic replacement	180.8 mA mg^{-1}	200 cycle	20
13	Pd-NiO-Y/CNT	Solid State dispersion	3-5 A/mg Pd	80000 s	This work

Cartesian coordinates of Fig. S13a

Pd	0.02429000	0.75880100	-0.09066000
O	1.37453400	-0.01069100	-1.29951300
O	1.63666500	0.79203800	1.00853400
O	-1.57409200	0.60408000	-1.20481300
O	-1.07319800	-0.39776200	1.03982800
Ni	2.70839500	-0.11587500	-0.08432500
O	4.39969900	0.41378200	-0.46109900
O	3.46016000	-1.69562700	0.38709600
Si	4.96121200	-1.07011400	0.03797300
O	5.94087200	-0.99344200	1.31381600
H	6.24710600	-1.80093700	1.73306700
O	5.73932000	-1.88059600	-1.11574100
H	6.57372300	-1.54927900	-1.45574100
Ni	-2.53295300	-0.31708800	0.00024700
O	-3.44562800	-1.81494800	-0.46077500
O	-4.12780600	0.27829500	0.62559800
Si	-4.84495600	-1.13193600	0.11851000
O	-5.97261500	-0.91361700	-1.01025400
H	-6.38202900	-1.67220600	-1.43277500
O	-5.52085000	-1.97274200	1.31417000
H	-6.28156500	-1.61801800	1.78009100
C	0.69851200	3.30291800	0.90587800
H	1.64264300	3.31933400	0.40264000
H	0.40653000	4.30640500	1.13535500
H	0.77350500	2.72492200	1.78335500
O	-0.29706500	2.68109900	0.08930000
H	-1.03020800	3.14740300	-0.31894200
H	-1.89941700	1.41472600	-0.80654600
O	-2.02732900	2.40475400	-0.71640100

Cartesian coordinates of Fig. S13b

Pd	-0.03118700	0.96446700	0.53543700
O	1.26975400	-0.07098300	-0.53724500
O	1.75103800	0.86695900	1.55102600
O	-1.82487300	0.83816500	-0.32219200
O	-0.93221200	-0.77177600	1.19197100
Ni	2.70766500	-0.11319000	0.51550200
O	4.16568300	0.27690400	-0.53335800
O	3.51861400	-1.76459500	0.48245200
Si	4.70978300	-1.28537400	-0.55289400
O	6.25501800	-1.48760000	-0.01889300
H	6.83413100	-1.99078800	-0.59610500
O	4.70884000	-2.02760000	-2.03376300
H	3.87253200	-2.04523400	-2.50746300
Ni	-2.46078000	-0.65963200	0.42540600
O	-3.41505000	-1.56141600	-0.87065600
O	-4.17665900	-0.31828400	1.00088700
Si	-4.87720800	-1.05816900	-0.29864500
O	-5.74116300	-0.06274800	-1.30492700
H	-5.28573600	0.71868700	-1.63132400
O	-5.95342000	-2.25526500	0.06265600
H	-6.81831000	-2.16711200	-0.34474100
C	1.63309800	3.32476900	-0.17762000
H	2.27269800	2.74656300	-0.85821600
H	1.56762900	4.35003700	-0.57004500
H	2.10883200	3.35107000	0.81029200
O	0.32677400	2.81688400	-0.13403800
H	-0.99356700	3.15678600	-1.56269400
H	-2.06405300	2.14500500	-1.82373500
O	-1.75571900	3.00504000	-2.14695000

Cartesian coordinates of Fig. S13c

Pd	0.10384	1.30667	0.0026
O	-1.06634	0.58298	1.41099
O	-1.65986	1.40693	-0.82709
O	1.85144	1.08548	0.84941
O	0.96307	0.11496	-1.28645
Ni	-2.57895	0.5349	0.42275
O	-4.16757	1.12665	1.06238
O	-3.45605	-1.01263	0.07802
Si	-4.85766	-0.3322	0.66009
O	-6.02344	-0.21173	-0.44437
H	-6.42303	-1.00482	-0.80898
O	-5.47367	-1.11836	1.92337
H	-6.2303	-0.75725	2.39103
Ni	2.57112	0.13465	-0.49153
O	3.48709	-1.39923	-0.17957
O	4.06841	0.67205	-1.36241
Si	4.80214	-0.76705	-0.97405
O	6.10196	-0.59763	-0.03856
H	6.54371	-1.37341	0.31445
O	5.24722	-1.62685	-2.26092
H	5.93755	-1.29897	-2.8419
C	-0.6773	4.00853	0.10262
H	-0.86332	3.9812	1.15597
H	-0.51698	5.0227	-0.19846
H	-1.4944	3.5895	-0.41356
O	0.46623	3.21623	-0.22791
H	-1.94738	2.3069	-0.91473
O	-2.21951	3.21479	-0.88679

Cartesian coordinates of Fig. S13d

Pd	0.10384	1.30667	0.0026
O	-1.06634	0.58298	1.41099
O	-1.65986	1.40693	-0.82709
O	1.85144	1.08548	0.84941
O	0.96307	0.11496	-1.28645
Ni	-2.57895	0.5349	0.42275
O	-4.16757	1.12665	1.06238
O	-3.45605	-1.01263	0.07802
Si	-4.85766	-0.3322	0.66009
O	-6.02344	-0.21173	-0.44437
H	-6.42303	-1.00482	-0.80898
O	-5.47367	-1.11836	1.92337
H	-6.2303	-0.75725	2.39103
Ni	2.57112	0.13465	-0.49153
O	3.48709	-1.39923	-0.17957
O	4.06841	0.67205	-1.36241
Si	4.80214	-0.76705	-0.97405
O	6.10196	-0.59763	-0.03856
H	6.54371	-1.37341	0.31445
O	5.24722	-1.62685	-2.26092
H	5.93755	-1.29897	-2.8419
C	-0.6773	4.00853	0.10262
H	-1.4944	3.5895	-0.41356
O	0.46623	3.21623	-0.22791
H	-1.94738	2.3069	-0.91473
O	-2.21951	3.21479	-0.88679
H	-0.69884	4.86122	0.74864

Cartesian coordinates of Fig. S14a

Pd	0.04568600	1.18735200	0.10514600
O	1.03277300	-0.34122100	-0.70634200
O	1.89871500	1.08612200	0.88724400
O	-1.84826700	1.14392400	-0.68178500
O	-0.99702900	-0.28651100	0.91378800
Ni	2.64677500	-0.22676200	-0.00212100
O	4.23803900	-0.17408100	-0.91739900
O	3.44114500	-1.68148400	0.76975500
Si	4.81692600	-1.49988000	-0.12759200
O	6.20697400	-1.13467100	0.69153100
H	6.59115800	-1.82500700	1.23691000
O	5.10509900	-2.85689200	-1.02527100
H	5.85201500	-2.84150400	-1.62813100
Ni	-2.59755100	-0.23686600	0.13924400
O	-3.06621400	-1.89028800	-0.47590500
O	-4.37777800	-0.18255500	0.58163500
Si	-4.63668100	-1.70198900	0.00270100
O	-5.79846400	-1.69762500	-1.17593300
H	-5.96740200	-2.52781800	-1.62773600
O	-5.04529700	-2.87334900	1.09880800
H	-5.92371800	-2.82193700	1.48299500
C	0.69827400	4.36040200	0.48306800
H	1.63187700	4.47914900	-0.07996900
H	0.09482600	5.26815200	0.35995200
H	0.95416700	4.24833200	1.54184800
O	-0.04809800	3.26826200	0.00963000
H	-1.08365300	3.47611800	-0.63912500
H	-2.23118400	2.61018700	-0.87106500
O	-2.00547300	3.49055200	-1.16998200

Cartesian coordinates of Fig. S14b

Pd	0.02479300	1.24548100	0.10346300
O	0.97016200	-0.39852900	-0.57476000
O	1.92043600	1.19973100	0.82942800
O	-1.85303000	1.06767700	-0.68079500
O	-0.96750500	-0.23987500	1.05277300
Ni	2.59298300	-0.20168700	0.04660600
O	4.11659000	-0.23095800	-0.98387600
O	3.46581600	-1.62749200	0.83134600
Si	4.75891100	-1.51431400	-0.17647200
O	6.20855400	-1.10450700	0.52000500
H	6.66727000	-1.77560700	1.02968900
O	4.96525900	-2.90717700	-1.05126100
H	5.68483500	-2.94349800	-1.68446600
Ni	-2.54513000	-0.22099400	0.24023000
O	-2.98281300	-1.86862800	-0.43000300
O	-4.35842200	-0.21806200	0.61737400
Si	-4.57620100	-1.70827700	-0.03468000
O	-5.65950800	-1.67160300	-1.28904600
H	-5.83001100	-2.48659500	-1.76530300
O	-5.02857500	-2.91349800	1.01483800
H	-5.93867600	-2.92432300	1.31777000
C	0.97954400	3.96705400	0.55480100
H	1.92290800	3.96228300	-0.00405000
H	0.59750600	4.99381600	0.61170800
H	1.18780900	3.60041700	1.56785800
O	0.02087400	3.17542700	-0.11312000
H	-1.38343200	3.64365100	-0.88002100
H	-2.56100500	2.72275800	-1.05277600
O	-2.22568200	3.62048700	-1.28087700

Cartesian coordinates of Fig. S14c

Pd	0.02471700	1.18058000	0.12789200
O	1.05050400	-0.41605800	-0.53305300
O	1.89703600	1.17187100	0.91307300
O	-1.87002600	1.01389000	-0.61460100
O	-0.99385600	-0.22419100	1.14353700
Ni	2.64617600	-0.21548700	0.17957300
O	4.09869600	-0.11921200	-0.94447500
O	3.60576800	-1.64979300	0.82351400
Si	4.82319200	-1.43273700	-0.26099000
O	6.31279100	-1.02181900	0.34304200
H	6.84592100	-1.72778500	0.71537400
O	5.01296500	-2.77555700	-1.21253100
H	5.71269700	-2.76200300	-1.86915800
Ni	-2.54344800	-0.29227800	0.34282900
O	-3.02560300	-1.81988400	-0.53298900
O	-4.34562700	-0.31593900	0.77758700
Si	-4.61262200	-1.68206900	-0.09026900
O	-5.70757600	-1.41425100	-1.30529700
H	-5.90761000	-2.14565000	-1.89361400
O	-5.09361800	-3.03478000	0.73961200
H	-6.02372400	-3.10329400	0.96607600
C	1.01978200	3.97544400	0.39859200
H	1.87456800	4.10774300	-0.27897000
H	0.56663400	4.95948500	0.58163400
H	1.40722500	3.57253300	1.34181700
O	0.05776400	3.14231700	-0.19650500
H	-1.71122000	3.74408200	-0.99216800
H	-2.84540300	2.80316700	-1.22556500
O	-2.62410400	3.74054200	-1.31711600

References

1. M. Sharma, M. Sharma, A. Hazarika, L. Satyanarayana, G. V. Karunakar and K. K. Bania, *Mol. Catal.,* 2017, **432**, 210–219.
2. X. Xu, X. Wang, S. Huo, Z. Chen, H. Zhao and J. Xu, *Catal. Today*, 2018, **318**, 157-166.
3. B. T. Sneed, C. N. Brodsky, C. H. Kuo, L. K. Lamontagne, Y. Jiang, Y. Wang, F. Tao, W. Huang and C. K. Tsung, *J. Am. Chem. Soc.*, 2013, **135**, 14691-14700.
4. M. J. Frisch, G. W. Trucks, H. B. Schlegel, et al., Gaussian 09, Revision B.01, Gaussian, Inc., Wallingford, CT, 2010.
5. Y. Wang, Q. He, J. Guo, H. Wei, K. Ding, H. Lin, S. Bhana, X. Huang, Z. Luo, T. D. Shen, S. Wei and Z. Guo, *ChemElectroChem*, 2015, **2**, 559–570.
6. C. Flores, V. L. Zholobenko, B. Gu, N. Batalha, V. Valtchev, W. Baaziz, O. Ersen, N. R. Marcilio, V. V. Ordomsky and A. Y. Khodakov, *ACS Appl. Nano Mater*., 2019, **27**, 4507-4517.
7. S. Fu, C. Zhu, Q. Shi, D. Dua and Y. Lin, *Catal. Sci. Technol*., 2016, **6**, 5052-5059.
8. (a) T. Sheng, J. Y. Ye, W. F. Lin and S. G. Sun, *Phys. Chem. Chem. Phys*., 2017, **19**, 7476-7480. (b) M. Sharma, B. Das, G. V. Karunakar, L. Satyanarayana and K. K. Bania, *J. Phys. Chem. C*, 2016, **120**, 13563-13573.
9. Y. C. Zhao, X. L. Yang, J. N. Tian, F. Y. Wang and L. Zhan, *Int. J. Hydrogen Energy*, 2010, **35**, 3249–3257.
10. J. Hu, X. Wu, Q. Zhang, M. Gao, H. Qiu, K. Huang, S. Feng, T. Wang, Y. Yang, Z. Liu and B. Zhao, *Langmuir*, 2018, **34**, 2685–2691.
11. Z. L. Liu, X. Zhang and L. Hong, *Electrochem. Commun*., 2009, **11**, 925-928.
12. Y. Song, X. Zhang, S. Yang, X. Wei and Z. Sun, *Fuel*, 2016, **181**, 269–276.
13. M. Zhang, Z. Yan and J. Xie, *Electrochim. Acta*, 2012, **77**, 237–243.
14. Z. Gu, H. Xu, D. Bin, B. Yan, S. Li, Z. Xiong, K. Zhang and Y. Du, *Colloids Surf. A*, 2017, **529**, 651–658.
15. Z. Qi, H. Geng, X. Wang, C. Zhao, H. Ji, C. Zhang, J. Xu and Z. Zhang, *J. Power Sources*, 2011, **196**, 5823–5828.
16. L. L. Carvalho, F. Colmati and A. A. Tanaka, *Int. J. Hydrogen, Energy*, 2017, **42**, 16118–16126.

17. J. Ju, Y. Shi and D. Wu, *Powder Technol*., 2012, **230**, 252-256.
18. R. S. Amin, R. M. A. Hameed, K. M. E. Khatib and M. E. Youssef, *Int. J. Hydrogen, Energy*, 2014, **39**, 2026-2041.
19. F. Miao, B. Tao, L. Sun, T. Liu, J. You, L. Wang and P. K. Chu, *J. Power Sources*, 2010, **195**, 146–150.
20. X. Niu, H. Zhao and M. Lan, *J. Power Sources*, 2016, **306**, 361-368.